ACS APPLIED MATERIALS & INTERFACES

Research Article

www.acsami.org

Tuning Two-Photon Photoluminescence of Gold Nanoparticle Aggregates with DNA and Its Application as Turn-on Photoluminescence Probe for DNA Sequence Detection

Peiyan Yuan, Rizhao Ma, Zhenping Guan, Nengyue Gao, and Qing-Hua Xu*

Department of Chemistry, National University of Singapore, 3 Science Drive 3, Singapore 117543

Supporting Information

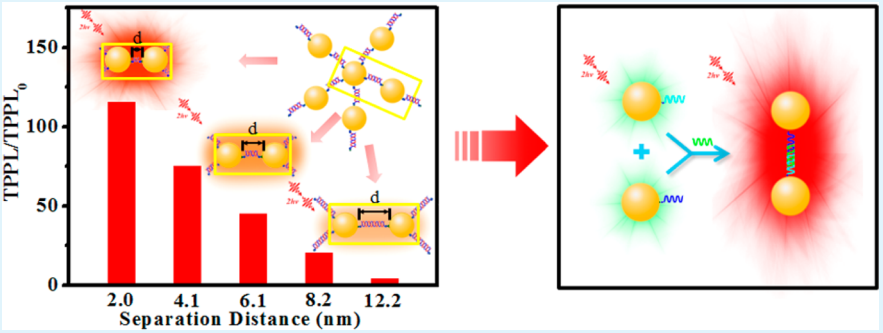

ABSTRACT: Plasmon coupling between noble metal nanoparticles has been known to dramatically enhance linear and nonlinear optical properties of nearby chromophores and metal nanoparticles themselves. The interparticle distance is expected to have significant influence on the coupling strength. Here we have prepared DNA tuned Au nanoparticle assemblies with well controlled separation distances from 2.0 to 12.2 nm to investigate plasmon coupling strength and particle size effects on two-photon photoluminescence (TPPL) enhancement. TPPL intensities of these DNA coupled nanoassemblies were found to increase rapidly as the separation distance decreases. The largest TPPL enhancement factors of 115 and 265 were achieved at the shortest available separation distance of 2.0 nm for 21 and 41 nm Au NPs-dsDNA assemblies, respectively. We have further utilized DNA induced coupling of Au NPs and TPPL enhancement to develop a two-photon sensing scheme for detection of DNA sequences. This TPPL based method displayed high sensitivity with a limit of detection of 2.9 pM and excellent selectivity against ssDNA with mismatched bases. A single mismatch can be easily differentiated at room temperature. Taking the unique advantages of two-photon excitation, this method could be potentially further extended to DNA detection inside cells or even in vivo. These findings can provide important insight for fundamental understanding of plasmon-coupling enhanced TPPL and development of various two-photon excitation based applications.

KEYWORDS: *gold nanoparticles, two-photon excitation, plasmon resonance, plasmon coupling, DNA detection, sensors*

1. INTRODUCTION

Noble metal nanoparticles, such as gold and silver, have been widely utilized in various biological and optoelectronic applications such as sensing, imaging, and phototherapy owing to their unique optical properties.[1−9] In particular, metal nanoparticles display localized surface plasmon resonance (LSPR) resulting from collective oscillation of electrons in the conduction band.[10,11] Wavelength and intensity of the LSPR band can be tuned by the particle size, shape, and dielectric properties of the surrounding medium as well as the plasmon coupling between the nanoparticles.[12−15] Plasmon coupling between neighboring nanoparticles has been known to significantly enhance the local electric field in the gap region.[16] Such properties have been widely utilized to enhance various linear and nonlinear optical properties such as surface-enhanced Raman scattering, one- and two-photon excitation fluorescence of nearby chromophores, and two-photon photoluminescence (TPPL) of metal nanoparticles themselves.[5,17−23] Plasmon coupling enhanced TPPL has potential applications in bioimaging, biosensing, and phototherapy due to the unique advantages of two-photon excitation, such as deep tissue penetration and localized excitation volume.[24−26] Gold nanoparticles (Au NPs) are attractive for biological applications due to their excellent chemical inertness and biocompatibility.[27,28] Plasmon coupling enhanced TPPL of Au NPs in colloid solutions and on substrates has been previously reported.[18,28−31] Schuck el al.[29] previously utilized lithographically fabricated Au bowties with a length of ∼75 nm and gaps of tens of nanometers and achieved enhancement of >10^3. Our recent work demonstrated TPPL enhancement of up to 10^5 for Au NPs at a separation distance of ∼1 nm on the single particle level.[18] The interparticle distance has been found to have

Received: May 15, 2014
Accepted: July 1, 2014
Published: July 1, 2014

significant influence on the coupling strength and TPPL intensities of metal nanoparticles on the substrates prepared by the electron beam lithography method.[29,30]

Electron beam lithography[21,29,30,32,33] and molecular bridge materials[15,27,31,34−40] are two typical methods to prepare nanostructures with precisely controlled interparticle separation distance. However, the electron beam lithography technique is expensive, complicated, and difficult to prepare nanostructures for applications in the form of colloid dispersions. Coupled nanostructures in the form of colloid dispersions offer more flexibility and versatility in biological applications compared to those on the substrates. Molecular bridge materials, such as polymers, bridged ligands, and DNA,[18,25,28,31,34−39] can be utilized to prepare colloid nanostructures with precisely controlled and much smaller separation distances in solution. Among various molecular bridge materials, DNA molecules are particularly attractive molecular bridge materials because of their selective-assembly, programmability, and controllable coupling distance.[39−41] A selective DNA induced nanoassembly could also be utilized for sensitive detection of DNA, which could provide useful information for identification of various diseases and pharmacogenomics.[42−44]

In this work, we report the preparation and TPPL properties of DNA coupled Au NP aggregates with well controlled interparticle separation distances from 2.0 to 12.2 nm. Au NP aggregates were prepared by hybridization of Au NPs modified with complementary ssDNA of different numbers of bases to form dsDNA of different strand lengths. Au NPs of two different sizes (21 and 41 nm) were utilized to systematically investigate the effect of the separation distance and nanoparticle size on TPPL properties of nanoparticle aggregates. Enhanced TPPL of DNA coupled Au NP assemblies has been further utilized to develop a TPPL turn on scheme for detection of DNA sequence, which displays high sensitivity as well as excellent selectivity over the noncomplementary DNA.

2. EXPERIMENTAL SECTION

Materials. Gold(III) chloride trihydrate ($HAuCl_4 \cdot 3H_2O$) and sodium citrate were obtained from Sigma and used as received without further purification. Milli-Q water was used in the experiments. All the oligonucleotides were purchased from Sigma. The sequences of different oligonucleotides are

D1: 5′-CGCGCTCTACTCTCGGATAGAAGAAATAGGAGTTA-$A(A)_{10}$-SH-3′

D2: 5′-TTAACTCCTATTTCTTCTATCCGAGAGTAGAGCGC-$G(A)_{10}$-SH-3′

D3: 5′-TTAACTCCTCTTTCTTCCATGCAA$(A)_{10}$-SH-3′

D4: 5′-TTGCATGGAAGAAAGAGGAGTTAA$(A)_{10}$-SH-3′

D5: 5′-TTAACTCCTCTTTCTTCC$(A)_{10}$-SH-3′

D6: 5′-GGAAGAAAGAGGAGTTAA$(A)_{10}$-SH-3′

D7: 5′-TTAACTCCTCTT$(A)_{10}$-SH-3′

D8: 5′-AAGAGGAGTTAA$(A)_{10}$-SH-3′

D9: 5′-TTAACT$(A)_{10}$-SH-3′

D10: 5′-AGTTAA$(A)_{10}$-SH-3′

D1 hybridizes with D2 to form a double stranded structure with 36 base pairs. D3 & D4, D5 & D6, D7 & D8, D9 & D10 hybridize to form double stranded structures with 24, 18, 12, and 6 base pairs, respectively.

Probe DNA_a: 5′-TCCATGCAACTCAAAAAAAAAA-SH-3′

Probe DNA_b: 5′-SH-AAAAAAAAAAAAGAGGAGTTAA -3′

Target DNA: 5′-GAGTTGCATGGATTAACTCCTCTT-3′

1-mismatched DNA: 5′-GAGTTGCATGGATTAACTTCTCTT-3′

2-mismatched DNA: 5′-GAGTTACATGGATTAACTTCTCTT-3′

3-mismatched DNA: 5′-GAGCTGCAAGGATTAACTTCTCTT-3′

Noncomplementary DNA: 5′-ACTTGGTGAAGCTAACGTTG-AGGC-3′

Preparation of 21 nm Gold Nanoparticles (Au NPs). Au NPs were prepared by reducing $HAuCl_4$ with sodium citrate, following a previously reported procedure.[36] Briefly, 507 μL of 10 mM $HAuCl_4$ was added into 18.5 mL of Mili-Q water. The mixture solution was heated to boiling. After 1.0 mL of 0.5 wt % sodium citrate was added, the solution turned pink in about 5 min. The obtained Au NPs had an average diameter of 20.6 ± 1.5 nm based on TEM images.

Preparation of 41 nm Au NPs. 41 nm Au NPs were prepared following a previous report.[34] 50 mL of 0.01 wt % $HAuCl_4$ solution was heated to 100 °C, followed by addition of 0.5 mL of 1 wt % sodium citrate solution. The resulting solution turned faintly blue in about 25 s and brilliant red within 70 s, indicating formation of Au NPs. The solution was kept boiling for 30 min. Au NPs with an average diameter of 41.0 ± 2.7 nm were obtained.

Preparation of Oligonucleotides-Modified Au NPs. Conjugation of ssDNA to Au NPs was performed based on a previously reported method.[38] Briefly, alkylthiol functionalized oligonucleotides (ssDNA-SH, sequence D1−D10) were first purified by using Nap-5 columns (GE Healthcare). 500 μL of Au NPs aqueous solution (1.28×10^{-10} M) was mixed with 50 μL of 20 μM thiol-modified oligonucleotides aqueous solution. This mixture solution was left >24 h for equilibration, followed by addition of 10 μL of phosphate buffered saline (PBS) buffer solution (100 mM phosphate, pH 7.4) and further addition of 15 μL of PBS twice at an interval of 4 h. After equilibration of at least 24 h, the solution was centrifuged at 12000 rpm for 20 min and then the supernatant was removed. The obtained precipitate was washed with PBS buffer (10 mM phosphate, pH 7.4) three times. The obtained ssDNA-Au NPs were redispersed into 250 μL of PBS buffer for transmission electron microscopy (TEM) measurements and subsequent experiments.

Hybridization of DNA-Modified Gold Nanoparticles. The 25 μL as-prepared complementary ssDNA(D_1)-Au NPs and ssDNA(D_2)-Au NPs (1.78×10^{-10} M in Au NPs) were mixed in 450 μL of PBS buffer solution (50 mM phosphate, pH 7.4) and kept at room temperature for 10 min for hybridization.

Detection of ssDNA. 25 μL of probe DNA_a-Au NPs and the probe DNA_b-Au NPs (1.78×10^{-10} M) were mixed in 450 μL of PBS buffer solution (50 mM phosphate, pH 7.4), followed by addition of different amounts of stock solution of the target DNA sequence. The mixture solutions were kept for 10 min before the measurements.

Characterizations and Instrumentations. Ultraviolet−visible (UV−vis) extinction spectra were taken by using a Shimadzu UV-2450 spectrophotometer. Transmission electron microscopy (TEM) images were taken on a JEOL 2010 transmission electron microscope. Dynamic light scattering (DLS) experiments were performed on a Malvern Nanosizer ZS instrument. An Avesta TiF-100 M femtosecond (fs) Ti:sapphire oscillator was used as the excitation source for TPPL measurements. The output laser pulses (pulse duration = 80 fs; repetition rate = 84.5 MHz) have a central wavelength of 820 nm. A lens with a focus length of 3.0 cm focused the laser beam onto the samples. The average excitation power before the sample is 100 mW. The emission was collected at an angle of 90° to the direction of the excitation beam and a 750 nm short pass filter was placed before the spectrometer to minimize the scattering. A monochromator (Acton Spectra Pro 2300i) coupled CCD (Princeton Instruments Pixis 100B) with an optical fiber was used to detect the emission signals.

3. RESULTS AND DISCUSSION

Citrate-stabilized Au NPs were prepared by following a previously reported method.[34,36] The obtained Au NPs are uniform with an average diameter of 20.6 ± 1.5 nm and LSPR band maximum at ∼520 nm (Figure 1). Thiol-modified ssDNA with different numbers of bases (5 pairs: 36, 24, 18, 12, and 6 bases) were utilized to functionalize the surface of Au NPs (the sequences of oligonucleotide strands are listed in the Experimental Section). The LSPR band of Au NPs displayed slight red shift after surface modification (Figure S1, Supporting

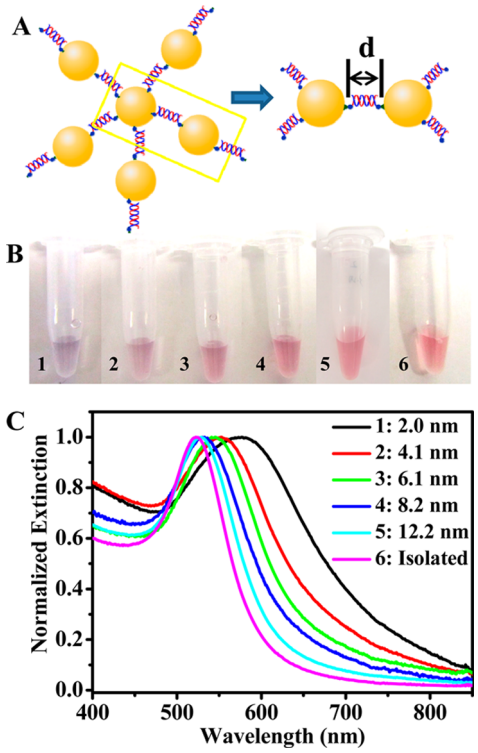

Figure 1. (A) Schematic structure, (B) photograph, and (C) normalized extinction spectra of 21 nm Au NPs-dsDNA assemblies with different separation distances (1, 2.0 nm; 2, 4.1 nm; 3, 6.1 nm; 4, 8.2 nm; 5, 12.2 nm; 6, isolated nanoparticles).

Information) due to the change in the refractive index of surface stabilizing agents.

dsDNA coupled Au NP assemblies were prepared by hybridization of two equal amounts of ssDNA modified Au NP samples with complementary base sequences in the PBS buffer solution (50 mM, pH 7.4). The nanoparticle separation distance was controlled by the number of base pairs in dsDNA. Assuming the length of each base pair in the double stranded structure is ~0.34 nm,[37,45] five different separation distances (12.2, 8.2, 6.1, 4.1, 2.0 nm) were obtained (Figure 1). Obvious color changes were observed after hybridization of two complementary Au NP-ssDNA samples (Figure 1B). The LSPR band was found to become red-shifted and broadened upon the hybridization (Figure 1C). The extent of red shift increased as the interparticle separation distance decreased, consistent with the previous simulation results.[34] The red shift can be ascribed to formation of a new plasmon coupling mode, which is sensitive to coupling strength. The coupling strength could be tuned by the interparticle distance. The broadening of the LSPR band is due to the formation of nanoparticle aggregates with different sizes such as trimers, tetramers, and even large aggregates. The formation of the Au NP assembly was further confirmed by transmission electron microscopy (TEM) images and dynamic light scattering (DLS) measurements (Figure S2, Supporting Information).

Coupled noble metal nanoparticles have been known to display significantly enhanced TPPL compared to uncoupled nanoparticles due due to enhanced two-photon excitation efficiency.[18,25,28,31] TPPL enhancement is expected to be strongly influenced by the coupling strength, which is dependent on the interparticle separation distance. To investigate the influence of interparticle separation distance, TPPL spectra of various dsDNA coupled Au NP aggregates were measured by using fs laser pulses at 820 nm as the excitation source. Figure 2 shows the TPPL spectra of dsDNA

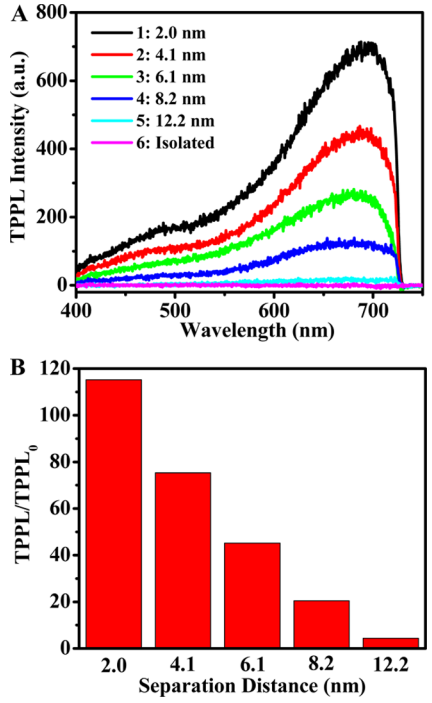

Figure 2. (A) TPPL spectra and (B) enhancement factors (TPPL/$TPPL_0$) of 21 nm Au NPs-dsDNA assembly with five different separation distances. $TPPL_0$ and TPPL are integrated TPPL intensities of DNA modified Au NPs before and after hybridization, respectively.

coupled Au NP aggregates with separation distances varying from 12.2 to 2.0 nm. The TPPL intensities of the dsDNA coupled Au NP aggregates were found to be significantly enhanced compared to that of unhybridized ssDNA modified ssDNA-Au NPs (Figure 2A). The TPPL enhancement factor (I_{TPPL}/I_{TPPL0}, where I_{TPPL0} and I_{TPPL} are the integrated TPPL intensities of DNA modified Au NPs before and after hybridization, respectively) increased rapidly as the separation distance decreased (Figure 2B). A maximum enhancement factor of up to 115-fold was obtained in the Au NPs assembly with smallest separation distance here (2.0 nm). The enhancement factor drops to 4.0-fold for Au NP assembly with separation distance of 12.2 nm. It needs to be noted that the observed TPPL enhancement factors for all the separation distances might be underestimated, as not all the ssDNA modified Au NPs hybridize to form assemblies. The observed enhancement factors were set as the lower limit of the optimum enhancement factors. The overall trend of the optimum enhancement factors will remain the same by assuming similar hybridization yields for different samples.

The local electric field enhancement of coupled metal nanoparticles has been known to depend on both the separation distance and nanoparticle size.[22,23,28,46] We have also examined the particle size effects on TPPL properties of Au NP assembly by performing similar experiments using Au NPs with diameters of 41.0 ± 2.7 nm and a LSPR band maximum at 527 nm (see TEM images and extinction spectra in Figure S3, Supporting Information). The extinction (Figure 3A) and TPPL spectra (Figure 3B) of the 41 nm Au NPs-dsDNA aggregates displayed a similar trend compared to that of the 21

dx.doi.org/10.1021/am502988u | ACS Appl. Mater. Interfaces 2014, 6, 13149−13156

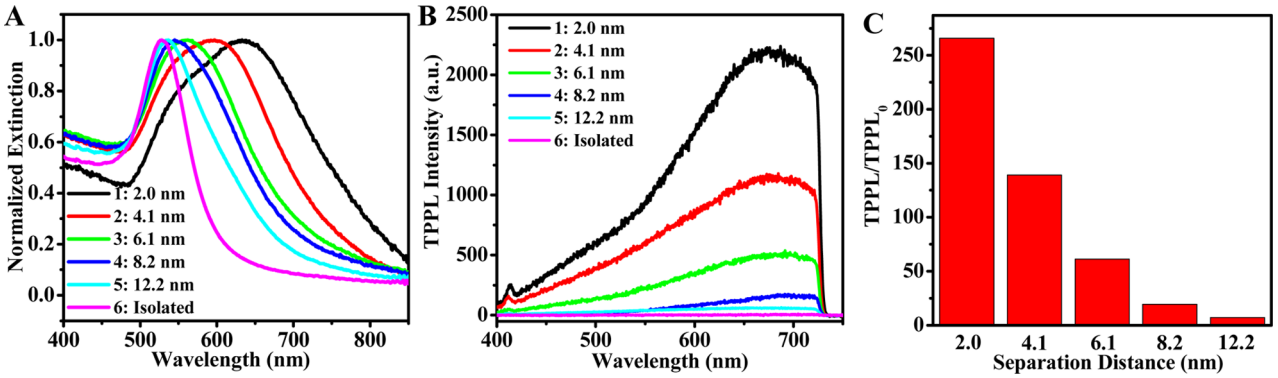

Figure 3. (A) Normalized extinction spectra, (B) TPPL spectra, and (C) TPPL enhancement factors of 41 nm Au NPs-dsDNA assembly with five different separation distances.

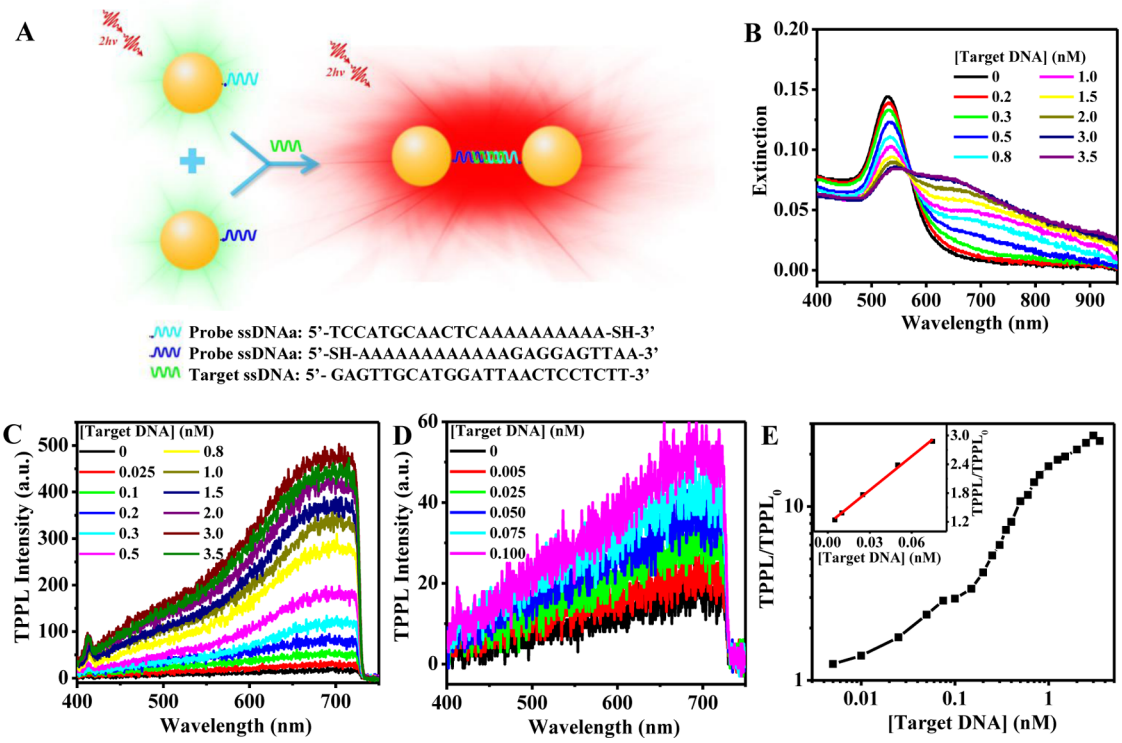

Figure 4. (A) Scheme for the two-photon sensing platform for detection of target ssDNA; (B, C, D) extinction spectra (B) and TPPL spectra (C, D) of $ssDNA_a$-Au NPs (41 nm) + $ssDNA_b$-Au NPs (41 nm) in the presence of different concentrations of target ssDNA; (E) TPPL enhancement factor versus different concentration of target ssDNA. The inset shows the linear plot in the low concentration range.

nm Au NPs-dsDNA aggregates. As the separation distance decreased, the LSPR band shifted to red and larger TPPL enhancement factor was observed. A maximum TPPL enhancement factor of 265-fold was obtained at the separation distance of 2.0 nm, which is larger than that of the 21 nm Au NP assembly (115-fold). The larger enhancement factor could be attributed to a stronger field enhancement in the coupling of NPs with a larger size.[47] The excitation power dependence of the TPPL intensities of 21 and 41 nm Au NPs-dsDNA aggregates (Figure S4, Supporting Information) indicated the emission intensities were approximately proportional to the square of the excitation power densities, which confirms involvement of two photons in the excitation process of the observed photoluminescence. Under fs laser excitation at 820 nm, we noticed some emission contribution for wavelength shorter than 410 nm. This shorter wavelength contribution likely arises from three-photon excitation, which was confirmed by the approximately cubic excitation power dependence of emission intensity from 380 to 400 nm (Figure S5, Supporting Information).

The observed TPPL enhancement can be ascribed to enhanced two-photon excitation efficiency due to formation of a new LSPR mode for resonance enhancement and enhanced local electric field at the excitation wavelength.[29,31,48,49] We have previously demonstrated that the excitation of TPPL from aggregated Au NPs involved two photons by two sequential one-photon absorption processes mediated by the intermediate states provided by the new LSPR mode.[50] The observation of larger enhancement at a shorter separation distance can be understood in terms of separation distance dependent coupling strength. A stronger coupling at a shorter separation distance[32−34,37] results in a red-shifted LSPR band with a larger extinction at the excitation wavelength (Figures 1C and 3A), which offers stronger resonance

dx.doi.org/10.1021/am502988u | ACS Appl. Mater. Interfaces 2014, 6, 13149−13156

enhancement and stronger electric field enhancement at the excitation wavelength, and consequently larger TPPL enhancement. Different from the large red shift in extinction spectra, the band maxima of TPPL spectra are located around 680−710 nm with only slight red shift for shorter separation distance (Figure S6, Supporting Information). This is due to inhomogeneous size distribution of the Au NP aggregates in the solution. We have previously showed that TPPL intensities of Au NP oligomers of different sizes and morphologies could differ by up to 5 orders of magnitude whereas the TPPL spectrum of each Au NP oligomer matches its corresponding extinction spectrum.[18,51] Au NP oligomers of different sizes and morphologies will thus contribute different weightages to the observed TPPL spectra of Au NP aggregates in colloid solution. The insensitivities of the TPPL spectral profile to the separation distance suggest that the observed TPPL in solution is dominated by Au NP oligomers with a LSPR band around 680−710 nm. We have measured the emission spectra of these Au NP assemblies by using continuous wave (CW) and fs laser excitation of the same average power at 820 nm. CW laser excitation did not give discernible emission signals, over 1000 times weaker than that under fs laser excitation (Figure S7, Supporting Information). The results suggest that the observed emission has very little contribution from one-photon excitation emission. We have further conducted TPPL measurements under fs laser excitation at three different wavelengths (780, 820, and 840 nm), which gave similar TPPL spectra profiles (Figure S8, Supporting Information). The insensitivity of the TPPL spectra profile to the excitation wavelength further excludes the possible contribution from scattered emission due to one-photon excitation and subsequent thermal excitation.

Plasmon coupling enhanced TPPL has been utilized to develop various highly sensitive and selective two-photon sensing platforms to take the unique advantages of two-photon excitation such as deep penetration in biological environment and potential in vivo detections.[25,52,53] DNA induced assembly of Au NPs and TPPL enhancement were further utilized to develop a two-photon sensing platform for DNA detection (Figure 4A). The single stranded DNA probes ($ssDNA_a$ and $ssDNA_b$, their sequences of oligonucleotide strands are listed in the Experimental Section) were separately modified onto the surface of 41 nm Au NPs. Upon addition of a target ssDNA, hybridization of three DNA strands (DNA_a, DNA_b and target DNA) allows formation of a 24-mer double stranded DNA coupled Au NPs assembly (with estimated coupling separation distance of 8.2 nm) as shown in Figure 4A. The solution changed color from red to reddish violet, which could be vaguely observed by naked eyes (observable for target ssDNA concentration higher than 0.3 nM). The target ssDNA induced Au NPs assembly could also be monitored by UV−vis extinction spectra (Figure 4B). As the concentration of target ssDNA increased, the original LSPR peak at 530 nm steadily decreased while a new LSPR peak appeared in the longer wavelength region. This new LSPR peak originated from the formed Au NPs-dsDNA aggregates. The extinction ratio $A_{650\ nm}/A_{530\ nm}$ could be utilized to quantitatively determine the concentration of target ssDNA (Figure S9, Supporting Information). The limit of detection (LOD) was estimated to be ∼0.15 nM based on the change in UV−vis extinction spectra. Formation of Au NPs-dsDNA aggregates could be confirmed by TEM images (Figure S10, Supporting Information).

The above observation of target ssDNA induced coupling between Au NPs-dsDNA could be further utilized to develop a two-photon DNA sensing scheme. TPPL spectra of $ssDNA_a$-Au NPs (41 nm) + $ssDNA_b$-Au NPs (41 nm) in the absence and presence of different concentrations of target ssDNA were measured by using 820 nm fs laser pulses as the excitation source. In the absence of target ssDNA, $ssDNA_a$-Au NPs (41 nm) + $ssDNA_b$-Au NPs (41 nm) exhibited a very weak TPPL signal, as there is no coupling between the ssDNA modified Au NPs. Upon addition of target ssDNA that induces the coupling between two types of Au NPs, TPPL intensity gradually increased with the increasing concentration of target ssDNA. TPPL intensity reached a maximum when the concentration of target ssDNA was 3 nM. The optimum enhancement factor was ∼25, which is consistent with that obtained from separation distance dependent TPPL for 41 nm Au NPs aggregates (Figure 3C) considering that 24-mer dsDNA gives a coupling separation distance of 8.2 nm. The strong correlation between TPPL enhancement factor and [ssDNA] could be utilized to quantitatively determine the concentration of target ssDNA. The Figure 4E inset shows that a linear dependence of TPPL enhancement on the concentration of target ssDNA at the low concentration range. In addition to broad dynamic detection range, this TPPL method offers highly sensitive detection of DNA with LOD as low as 2.9 pM, which was significantly lower than the LOD of many other reported methods (∼10 pM-1 nM).[42,44,54−56]

This two-photon detection method also showed high selectivity against DNA sequences with mismatched bases. The selectivity of this TPPL based method was tested by measuring TPPL of $ssDNA_a$-Au NPs (41 nm) + $ssDNA_b$-Au NPs (41 nm) in the presence of 1.5 nM DNA sequences with different numbers of mismatched bases at room temperature (20 °C) (Figure 5). The corresponding UV−vis extinction spectra of the samples are shown in Figure S11 (Supporting Information). It can be seen that TPPL intensity steadily decreased with the increasing number of mismatched base pairs in the detected DNA strands. TPPL intensity of the Au NPs-dsDNA aggregates with one base pair mismatch is distinctly different from that with the fully complementary DNA strand. Single base pair mismatch could be easily detected at room temperature.

Similar to the colorimetric methods,[38] a potential limitation of this TPPL method is very weak plasmon coupling at large separation distances, which results in significantly reduced TPPL intensities. The sensitivity of the TPPL method for detection of DNA sequences with a very large number of bases will decrease if smaller Au NPs were used. As our experiments have shown, coupling of larger Au NPs at larger separation distances still gave reasonable TPPL enhancement. This limitation for detection of longer DNA strands could be overcome by using larger sized Au NPs to improve its detection sensitivity or combining with other methods to cleave the longer stranded DNA to shorter DNA strands before the detection.[57−59]

4. SUMMARY

In this work, we have prepared dsDNA coupled Au NPs aggregates with well controlled separation distances varying from 2.0 to 12.2 nm by using dsDNA of different numbers of base pairs. Red shifted LSPR band and significantly enhanced TPPL intensities were observed at shorter separation distances. The largest TPPL enhancement factors are 115 and 265 at the

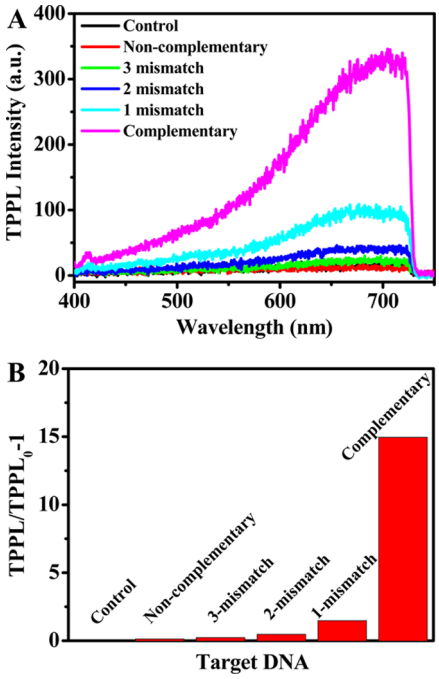

Figure 5. (A) TPPL spectra (B) TPPL enhancement factors of $ssDNA_a$-Au NPs (41 nm) + $ssDNA_b$-Au NPs (41 nm) before (the control sample) and after addition of 1.5 nM target DNA, 1-mismatched, 2-mismatched, 3-mismatched, and noncomplementary DNA.

shortest available separation distance of 2.0 nm for 21 and 41 nm Au NPs-dsDNA aggregates, respectively. These findings can provide important insight for fundamental understanding of plasmon-coupling enhanced TPPL and development of various two-photon excitation based applications. We have further utilized DNA induced coupling of Au NPs and TPPL enhancement to develop a two-photon sensing scheme for detection of DNA sequences. This TPPL based method displayed high sensitivity with a LOD of 2.9 pM and excellent selectivity against ssDNA with mismatched bases. A single mismatch could be easily differentiated at room temperature. Taking the unique advantages of two-photon excitation such as deep tissue penetration and 3-dimensional mapping, this method could be potentially further extended to detection of target ssDNA inside cells or even in vivo.

■ ASSOCIATED CONTENT

Supporting Information

TEM images, extinction spectra, and dynamic light scattering data of 21 nm Au NPs before and after DNA induced coupling; TEM images and extinction spectra of 41 nm Au NPs; excitation power dependence of the TPPL of Au NPs-dsDNA aggregates; Normalized TPPL spectra of Au NPs-dsDNA assemblies with five different separation distances; PL spectra of Au NP assemblies under CW and fs laser excitation of the same average power; excitation wavelength dependent TPPL spectra of the Au NPs-dsDNA assembly; extinction ratio $A_{650\ nm}/A_{530\ nm}$ and TEM images of probes ssDNA-Au NPs in the absence and presence of target ssDNA; extinction spectra of the samples for selectivity test. This material is available free of charge via the Internet at http://pubs.acs.org.

■ AUTHOR INFORMATION

Corresponding Author

*Q.-H. Xu. E-mail: chmxqh@nus.edu.sg.

Notes

The authors declare no competing financial interest.

■ ACKNOWLEDGMENTS

This research is supported by DSTA Singapore (Project DSTA-NUS-DIRP/9010100347) and the National Research Foundation, Prime Minister's Office, Singapore under its Competitive Research Program (CRP Award No. NRF-CRP10-2012-04).

■ REFERENCES

(1) Song, S.; Qin, Y.; He, Y.; Huang, Q.; Fan, C.; Chen, H.-Y. Functional Nanoprobes for Ultrasensitive Detection of Biomolecule. *Chem. Soc. Rev.* **2010**, *39*, 4234−4243.

(2) Hu, M.; Chen, J.; Li, Z.-Y.; Au, L.; Hartland, G. V.; Li, X.; Marquez, M.; Xia, Y. Gold Nanostructures: Engineering Their Plasmonic Properties for Biomedical Applications. *Chem. Soc. Rev.* **2006**, *35*, 1084−1094.

(3) Xu, X.; Han, M. S.; Mirkin, C. A. A Gold-Nanoparticle-Based Real-Time Colorimetric Screening Method for Endonuclease Activity and Inhibition. *Angew. Chem., Int. Ed.* **2007**, *119*, 3538−3540.

(4) Chen, J. I. L.; Chen, Y.; Ginger, D. S. Plasmonic Nanoparticle Dimers for Optical Sensing of DNA in Complex Media. *J. Am. Chem. Soc.* **2010**, *132*, 9600−9601.

(5) Zhao, T.; Yu, K.; Li, L.; Zhang, T.; Guan, Z.; Gao, N.; Yuan, P.; Li, S.; Yao, S. Q.; Xu, Q.-H.; Xu, G. Q. Gold Nanorod Enhanced Two-Photon Excitation Fluorescence of Photosensitizers for Two-Photon Imaging and Photodynamic Therapy. *ACS Appl. Mater. Interfaces* **2014**, *6*, 2700−2708.

(6) Liu, J.; Lu, Y. Fast Colorimetric Sensing of Adenosine and Cocaine Based on a General Sensor Design Involving Aptamers and Nanoparticles. *Angew. Chem., Int. Ed.* **2006**, *118*, 96−100.

(7) Li, J. L.; Day, D.; Gu, M. Ultra-Low Energy Threshold for Cancer Photothermal Therapy Using Transferrin-Conjugated Gold Nanorods. *Adv. Mater.* **2008**, *20*, 3866−3871.

(8) Imura, K.; Nagahara, T.; Okamoto, H. Plasmon Mode Imaging of Single Gold Nanorods. *J. Am. Chem. Soc.* **2004**, *126*, 12730−12731.

(9) Wang, J.; Wang, L.; Liu, X.; Liang, Z.; Song, S.; Li, W.; Li, G.; Fan, C. A Gold Nanoparticle-Based Aptamer Target Binding Readout for ATP Assay. *Adv. Mater.* **2007**, *19*, 3943−3946.

(10) Link, S.; El-Sayed, M. A. Optical Properties and Ultrafast Dynamics in Metallic Nanocrystals. *Annu. Rev. Phys. Chem.* **2003**, *54*, 331−366.

(11) Bohren, C. F.; Huffman, D. R. *Absorption and Scattering of Light by Small Particles*; Wiley: New York, 1983.

(12) Chen, H.; Ming, T.; Zhao, L.; Wang, F.; Sun, L.-D.; Wang, J.; Yan, C.-H. Plasmon-Molecule Interactions. *Nano Today* **2010**, *5*, 494−505.

(13) Noguez, C. Surface Plasmons on Metal Nanoparticles: The Influence of Shape and Physical Environment. *J. Phys. Chem. C* **2007**, *111*, 3806−3819.

(14) Yeshchenko, O. A.; Dmitruk, I. M.; Alexeenko, A. A.; Losytskyy, M. Y.; Kotko, A. V.; Pinchuk, A. O. Size-Dependent Surface-Plasmon-Enhanced Photoluminescence from Silver Nanoparticles Embedded in Silica. *Phys. Rev. B* **2009**, *79*, 235438.

(15) Zheng, Y. B.; Kiraly, B.; Cheunkar, S.; Huang, T. J.; Weiss, P. S. Incident-Angle-Modulated Molecular Plasmonic Switches: A Case of Weak Exciton−Plasmon Coupling. *Nano Lett.* **2011**, *11*, 2061−2065.

(16) Nie, S.; Emory, S. R. Probing Single Molecules and Single Nanoparticles by Surface-Enhanced Raman Scattering. *Science* **1997**, *275*, 1102−1106.

(17) Chen, D.; Xu, Q.-H. Separation Distance Dependent Fluorescence Enhancement of Fluorescein Isothiocyanate by Silver Nanoparticles. *Chem. Commun.* **2007**, 248−250.

(18) Guan, Z.; Gao, N.; Jiang, X.-F.; Yuan, P.; Han, F.; Xu, Q.-H. Huge Enhancement in Two-Photon Photoluminescence of Au Nanoparticle Clusters Revealed by Single-Particle Spectroscopy. *J. Am. Chem. Soc.* **2013**, *135*, 7272−7277.
(19) Bardhan, R.; Grady, N. K.; Cole, J. R.; Joshi, A.; Halas, N. J. Fluorescence Enhancement by Au Nanostructures: Nanoshells and Nanorods. *ACS Nano* **2009**, *3*, 744−752.
(20) Fang, Z.; Fan, L.; Lin, C.; Zhang, D.; Meixner, A. J.; Zhu, X. Plasmonic Coupling of Bow Tie Antennas with Ag Nanowire. *Nano Lett.* **2011**, *11*, 1676−1680.
(21) Kinkhabwala, A.; Yu, Z. F.; Fan, S. H.; Avlasevich, Y.; Mullen, K.; Moerner, W. E. Large Single-Molecule Fluorescence Enhancements Produced by a Bowtie Nanoantenna. *Nat. Photonics* **2009**, *3*, 654−657.
(22) Xu, H.; Aizpurua, J.; Käll, M.; Apell, P. Electromagnetic Contributions to Single-Molecule Sensitivity in Surface-Enhanced Raman Scattering. *Phys. Rev. E* **2000**, *62*, 4318−4324.
(23) Genov, D. A.; Sarychev, A. K.; Shalaev, V. M.; Wei, A. Resonant Field Enhancements from Metal Nanoparticle Arrays. *Nano Lett.* **2003**, *4*, 153−158.
(24) Narayanan, A.; Varnavski, O. P.; Swager, T. M.; Goodson, T. Multiphoton Fluorescence Quenching of Conjugated Polymers for TNT Detection. *J. Phys. Chem. C* **2008**, *112*, 881−884.
(25) Jiang, C.; Guan, Z.; Lim, S. Y. R.; Polavarapu, L.; Xu, Q.-H. Two-photon Ratiometric Sensing of Hg^{2+} by Using Cysteine Functionalized Ag Nanoparticles. *Nanoscale* **2011**, *3*, 3316−3320.
(26) Kim, H. M.; Seo, M. S.; An, M. J.; Hong, J. H.; Tian, Y. S.; Choi, J. H.; Kwon, O.; Lee, K. J.; Cho, B. R. Two-Photon Fluorescent Probes for Intracellular Free Zinc Ions in Living Tissue. *Angew. Chem., Int. Ed.* **2008**, *120*, 5245−5248.
(27) Llevot, A.; Astruc, D. Applications of Vectorized Gold Nanoparticles to the Diagnosis and Therapy of Cancer. *Chem. Soc. Rev.* **2012**, *41*, 242−257.
(28) Han, F.; Guan, Z.; Tan, T. S.; Xu, Q.-H. Size-Dependent Two-Photon Excitation Photoluminescence Enhancement in Coupled Noble-Metal Nanoparticles. *ACS Appl. Mater. Interfaces* **2012**, *4*, 4746−4751.
(29) Schuck, P. J.; Fromm, D. P.; Sundaramurthy, A.; Kino, G. S.; Moerner, W. E. Improving the Mismatch between Light and Nanoscale Objects with Gold Bowtie Nanoantennas. *Phys. Rev. Lett.* **2005**, *94*, 017402.
(30) Ueno, K.; Juodkazis, S.; Mizeikis, V.; Sasaki, K.; Misawa, H. Clusters of Closely Spaced Gold Nanoparticles as a Source of Two-Photon Photoluminescence at Visible Wavelengths. *Adv. Mater.* **2008**, *20*, 26−30.
(31) Guan, Z.; Polavarapu, L.; Xu, Q.-H. Enhanced Two-Photon Emission in Coupled Metal Nanoparticles Induced by Conjugated Polymers. *Langmuir* **2010**, *26*, 18020−18023.
(32) Sundaramurthy, A.; Crozier, K. B.; Kino, G. S.; Fromm, D. P.; Schuck, P. J.; Moerner, W. E. Field Enhancement and Gap-Dependent Resonance in a System of Two Opposing Tip-to-Tip Au Nanotriangles. *Phys. Rev. B* **2005**, *72*, 165409.
(33) Fromm, D. P.; Sundaramurthy, A.; Schuck, P. J.; Kino, G.; Moerner, W. E. Gap-Dependent Optical Coupling of Single "Bowtie" Nanoantennas Resonant in the Visible. *Nano Lett.* **2004**, *4*, 957−961.
(34) Zhong, Z.; Patskovskyy, S.; Bouvrette, P.; Luong, J. H. T.; Gedanken, A. The Surface Chemistry of Au Colloids and Their Interactions with Functional Amino Acids. *J. Phys. Chem. B* **2004**, *108*, 4046−4052.
(35) Sardar, R.; Heap, T. B.; Shumaker-Parry, J. S. Versatile Solid Phase Synthesis of Gold Nanoparticle Dimers Using an Asymmetric Functionalization Approach. *J. Am. Chem. Soc.* **2007**, *129*, 5356−5357.
(36) Cho, E. C.; Choi, S.-W.; Camargo, P. H. C.; Xia, Y. Thiol-Induced Assembly of Au Nanoparticles into Chainlike Structures and Their Fixing by Encapsulation in Silica Shells or Gelatin Microspheres. *Langmuir* **2010**, *26*, 10005−10012.
(37) Busson, M. P.; Rolly, B.; Stout, B.; Bonod, N.; Larquet, E.; Polman, A.; Bidault, S. Optical and Topological Characterization of Gold Nanoparticle Dimers Linked by a Single DNA Double Strand. *Nano Lett.* **2011**, *11*, 5060−5065.
(38) Elghanian, R.; Storhoff, J. J.; Mucic, R. C.; Letsinger, R. L.; Mirkin, C. A. Selective Colorimetric Detection of Polynucleotides Based on the Distance-Dependent Optical Properties of Gold Nanoparticles. *Science* **1997**, *277*, 1078−1081.
(39) Lee, J. H.; Wernette, D. P.; Yigit, M. V.; Liu, J.; Wang, Z.; Lu, Y. Site-Specific Control of Distances between Gold Nanoparticles Using Phosphorothioate Anchors on DNA and a Short Bifunctional Molecular Fastener. *Angew. Chem., Int. Ed.* **2007**, *119*, 9164−9168.
(40) Lim, D.-K.; Jeon, K.-S.; Hwang, J.-H.; Kim, H.; Kwon, S.; Suh, Y. D.; Nam, J.-M. Highly Uniform and Reproducible Surface-Enhanced Raman Scattering from DNA-Tailorable Nanoparticles with 1-nm Interior Gap. *Nat. Nanotechnol.* **2011**, *6*, 452−460.
(41) Lee, J.-H.; Kim, G.-H.; Nam, J.-M. Directional Synthesis and Assembly of Bimetallic Nanosnowmen with DNA. *J. Am. Chem. Soc.* **2012**, *134*, 5456−5459.
(42) He, S.; Liu, K.-K.; Su, S.; Yan, J.; Mao, X.; Wang, D.; He, Y.; Li, L.-J.; Song, S.; Fan, C. Graphene-Based High-Efficiency Surface-Enhanced Raman Scattering-Active Platform for Sensitive and Multiplex DNA Detection. *Anal. Chem.* **2012**, *84*, 4622−4627.
(43) McCarthy, J. J.; Hilfiker, R. The Use of Single-Nucleotide Polymorphism Maps in Pharmacogenomics. *Nat. Biotechnol.* **2000**, *18*, 505−508.
(44) Mancuso, M.; Jiang, L.; Cesarman, E.; Erickson, D. Multiplexed Colorimetric Detection of Kaposi's Sarcoma Associated Herpesvirus and Bartonella DNA Using Gold and Silver Nanoparticles. *Nanoscale* **2013**, *5*, 1678−1686.
(45) Marie, R.; Pedersen, J. N.; Bauer, D. L. V.; Rasmussen, K. H.; Yusuf, M.; Volpi, E.; Flyvbjerg, H.; Kristensen, A.; Mir, K. U. Integrated View of Genome Structure and Sequence of a Single DNA Molecule in a Nanofluidic Device. *Proc. Natl. Acad. Sci. U. S. A.* **2013**, *110*, 4893−4898.
(46) Hao, E.; Schatz, G. C. Electromegnetic Fields around Silver Nanoparticles and Dimers. *J. Chem. Phys.* **2004**, *120*, 357−366.
(47) Marinica, D. C.; Kazansky, A. K.; Nordlander, P.; Aizpurua, J.; Borisov, A. G. Quantum Plasmonics: Nonlinear Effects in the Field Enhancement of a Plasmonic Nanoparticle Dimer. *Nano Lett.* **2012**, *12*, 1333−1339.
(48) Biagioni, P.; Celebrano, M.; Savoini, M.; Grancini, G.; Brida, D.; Mátéfi-Tempfli, S.; Mátéfi-Tempfli, M.; Duò, L.; Hecht, B.; Cerullo, G.; Finazzi, M. Dependence of the Two-Photon Photoluminescence Yield of Gold Nanostructures on the Laser Pulse Duration. *Phys. Rev. B* **2009**, *80*, 045411.
(49) Ghenuche, P.; Cherukulappurath, S.; Taminiau, T. H.; van Hulst, N. F.; Quidant, R. Spectroscopic Mode Mapping of Resonant Plasmon Nanoantennas. *Phys. Rev. Lett.* **2008**, *101*, 116805.
(50) Jiang, X.-F.; Pan, Y.; Jiang, C.; Zhao, T.; Yuan, P.; Venkatesan, T.; Xu, Q.-H. Excitation Nature of Two-Photon Photoluminescence of Gold Nanorods and Coupled Gold Nanoparticles Studied by Two-Pulse Emission Modulation Spectroscopy. *J. Phys. Chem. Lett.* **2013**, *4*, 1634−1638.
(51) Gao, N.; Chen, Y.; Li, L.; Guan, Z.; Zhao, T.; Zhou, N.; Yuan, P.; Yao, S. Q.; Xu, Q.-H. Shape-Dependent Two-Photon Photoluminescence of Single Gold Nanoparticles. *J. Phys. Chem. C* **2014**, *118*, 13904−13911.
(52) Guan, Z.; Li, S.; Cheng, P. B. S.; Zhou, N.; Gao, N.; Xu, Q.-H. Band-Selective Coupling-Induced Enhancement of Two-Photon Photoluminescence in Gold Nanocubes and Its Application as Turn-on Fluorescent Probes for Cysteine and Glutathione. *ACS. Appl. Mater. Interfaces* **2012**, *4*, 5711−5716.
(53) Jiang, C.; Zhao, T.; Li, S.; Gao, N.; Xu, Q.-H. Two-Photon Induced Photoluminescence and Singlet Oxygen Generation from Aggregated Gold Nanoparticles. *ACS. Appl. Mater. Interfaces* **2013**, *5*, 10853−10857.
(54) Kwon, S. J.; Bard, A. J. DNA Analysis by Application of Pt Nanoparticle Electrochemical Amplification with Single Label Response. *J. Am. Chem. Soc.* **2012**, *134*, 10777−10779.

(55) Fong, K. E.; Yung, L.-Y. L. Head-to-Tail: Hybridization and Single-Mismatch Discrimination in Metallic Nanoparticle−DNA Assembly. *RSC Adv.* **2013**, *3*, 6076−6084.
(56) Liu, M.; Wang, Z.; Zong, S.; Zhang, R.; Zhu, D.; Xu, S.; Wang, C.; Cui, Y. SERS-Based DNA Detection in Aqueous Solutions Using Oligonuclcotide-Modified Ag Nanoprisms and Gold Nanopartilces. *Anal. Bioanal. Chem.* **2013**, *405*, 6131−6136.
(57) Shen, Q.; Zhou, N.; Guo, M.; Zhong, C.-J.; Lin, B.; Li, W.; Yao, S. Simple and Rapid Colorimetric Sensing of Enzymatic Cleavage and Oxidative Damage of Single-Stranded DNA with Unmodified Gold Nanoparticles Asindicator. *Chem. Commun.* **2009**, 929−931.
(58) Feng, F.; Tang, Y.; He, F.; Yu, M.; Duan, X.; Wang, S.; Li, Y.; Zhu, D. Fast Cationic Conjugated Polymer/DNA Complexes for Amplified Fluorescence Assays of Nucleases and Methyltransferases. *Adv. Mater.* **2007**, *19*, 3490−3495.
(59) Tang, Y.; Feng, F.; He, F.; Wang, S.; Li, Y.; Zhu, D. Direct Visualization of Enzymatic Cleavage and Oxidative Damage by Hydroxyl Radicals of Single-Stranded DNA with a Cationic Polythiophene Derivative. *J. Am. Chem. Soc.* **2006**, *128*, 14972−14976.